Large-time response of ice cover to a load moving along a frozen channel

Tatyana Khabakhpasheva[a], Konstantin Shishmarev[b,*], Alexander Korobkin[c]

[a]*Lavrentyev Institute of Hydrodynamics, Novosibirsk, Russia*
[b]*Altai State University, Barnaul, Russia*
[c]*School of Mathematics, University of East Anglia, Norwich, UK*

Abstract

Unsteady response of an ice cover in a channel with vertical walls is studied for large times. The ice deflection is caused by a load moving along the frozen channel at a constant speed. The ice cover is modelled as a thin elastic plate clamped to the walls of the channel. The time-dependent problem is solved by using the Fourier transform along the channel and the method of separating variables. In the system moving along the channel together with the load, the large-time deflection of the ice cover consists of steady deflection and standing waves in front and behind the load. The number of waves, their frequencies and wavenumbers depend on the speed of the load and the values of the critical speeds for the channel. The number of the waves and their amplitudes are calculated for a given load and its speed. The maximum stress in the ice as a function of the load speed is estimated.

Keywords: Elastic plate, Moving loads, Ice defections and strains, Large time behaviour

1. Introduction

The ice responses to loads moving along an unbounded ice cover are well studied for water of both infinite and constant depth (see an excellent review in [1]) by using the linear theory of hydroelasticity. It is known that the ice response strongly depends on the speed of the load. If the speed is below a certain critical value, the ice deflection is localized near the load and quickly decays with the distance from the load. For higher speeds of the load, outgoing waves are formed in the far field if viscous damping in the ice is small and not included in the mathematical model. At the critical speed, the linear theory of hydroelasticity without damping predicts unbounded ice response. To obtain estimates of the ice response for the critical speed of the load, either non linear effects [2] or viscous damping [3], or both are included in the ice model.

Viscoelastic models of the sea ice were studied by Tabata [4]. He performed experiments with rectangular floating ice beams under given loads to obtain the bending stresses as functions of time. By analysing the measured stresses Tabata concluded that viscoelastic properties of the ice are well described by a rheological model with a Maxwell unit and a Voigt (Kelvin) unit connected in series. The model includes four parameters. A two-parameter viscoelastic model of ice was used by Hosking et al. [3]. The Maxwell and Kelvin-Voigt models of viscoelastic ice were employed in [5], where the theoretical predictions of ice response within these two viscoelastic models and their combinations were compared to available experimental results with moving

---

loads. It was shown that a simple one-parameter model with a retardation time τ, the so-called Kelvin-Voigt model, gives very reasonable results, see [5] and [6]. The retardation time is difficult to determine. In experiments [6], the retardation time varied from 3 to 10 seconds, in order to approximate the measured deflections for different loadings. Note that the water viscosity gives negligible contribution to the damping of ice response for channels with dimensions of order of a metre and load speeds of order of several metres per second.

The presence of walls and obstacles complicates the problem of moving loads. There are many critical speeds for a frozen channel, in contrast to the ice sheet of infinite extent with just two critical values of the load speed [7]. Each critical speed for an ice cover in a channel corresponds to a mode of hydroelastic wave propagating along the channel with a certain profile across the channel and its own dispersion relation. These waves were studied by Korobkin et al. [7]. The problem of a load moving along a frozen channel was studied in [8] within the Kelvin-Voigt viscoelastic model of the ice cover. The steady state solution of the problem was derived in the coordinate system moving together with the load. This approach does not require initial data. The problem was solved numerically. Both the deflection and strain distributions in the ice plate were investigated. The deflections and strains quickly decay with the distance from the load within the viscoelastic ice model. The rate of decay is related to the retardation time τ. This is correct even for small values of the retardation time. The value $\tau = 0.1$ s was used in most of the calculations performed in [8]. The effects of the channel width, the ice thickness and the speed of the load on the ice response were studied. Both deflections and strains were given by infinite series and integrals. Decreasing viscous damping, higher strains in the ice cover and longer region of significant deflections along the channel were obtained for speeds of the load different from the critical values. Numerical integration was challenging for small damping. Small values of the retardation time could lead to inaccurate results. To estimate the strains accurately, we need to know them for zero damping, where the approach of [8] does not work.

Another approach to estimating the stationary response of ice cover to a load moving steadily along a frozen channel is used in this paper. This approach was introduce in [9] for a load moving along an ice plate of infinite extent. The approach does not rely on a viscoelastic model of ice. Models of ice response without damping are less physical. However, they may provide helpful estimates of maximum strains and bearing capacity of the ice cover. The ice cover is modelled as an elastic thin plate of constant thickness. In this model, stationary ice response is obtained as the limit of unsteady solution for large times. At $t = 0$ the load, which is modelled by an external localised pressure over the ice plate, is at rest. The initial ice deflection satisfies the stationary equation of thin elastic plate with corresponding boundary conditions on the walls of the channel. The external pressure is symmetric with respect to the central line of the channel in the present study. Then the load starts to move at a constant speed U along the channel. The ice deflection decays far ahead and far behind the moving load for finite times. The resulting problem of unsteady linear hydroelasticity is solved in this paper by using the Fourier transform along the channel and the normal-mode method, see [10], [11], [12], for the ice deflection. Second-order differential equations in time for the principal coordinates of the normal modes are derived and solved analytically. As a result, the ice deflection is presented by an infinite series of regular Fourier integrals. The limiting values of the integrals as $t \to \infty$,

in the coordinate system moving together with the load, are obtained by the asymptotic methods similar to those used in [9]. The limiting values of the integrals depend on the speed of the load with respect to the critical speeds of the propagating-sloshing waves along the channel. It is shown that for large times the total ice deflection consists of symmetric deflection localized near the load and a system of waves in front and behind the load. The number of these waves is obtained and the wave amplitudes are evaluated numerically. Each wave propagates along the channel with the speed of the load U. The waves are stationary in the coordinate system moving together with the load.

This study is motivated by experiments in ice tanks, operations on ice in rivers and channels such as cargo transportation or ice breaking to avoid flooding, and ice-structure interaction. The strains calculated with zero damping are higher than the real ones. For safe transportation on ice, one needs to compare the computed strains with a strain critical value, and determine safe conditions of transportation. By using the computed amplitudes of the waves generated by the moving load, we can find places of the highest strains far ahead and behind the load and estimate their values. It can be expected that there are such speeds of the load that the maximum strains behind and/or in front of the load are achieved at the walls of the channel, see [7]. It is possible also that the yield strain value is achieved in the waves in front of the moving load. Then the load moves actually along the broken ice in the channel or along the plate detached from the channel walls, see [13].

The problem formulation and general assumptions are given in Section 2. The method of solution by using the Fourier transform and normal mode decomposition is presented in Section 3. Numerical results are reported and discussed in Section 4. The conclusions are drawn in Section 5.

2. Formulation of the problem

The unsteady hydroelastic waves generated by a load moving along a channel covered with ice are considered in the Cartesian coordinates x, y, z. The channel is of rectangular cross section with finite depth H, $-H < z < 0$, and width $2L$, $-L < y < L$, see Figure 1. The channel is infinitely long, $-\infty < x < \infty$, and occupied with an incompressible and inviscid liquid of density ρ_l. The liquid is covered with an ice plate of density ρ_i, constant thickness h_i, and rigidity $D = Eh_i^3/[12(1 - \nu^2)]$, where E is the Young's modulus of the ice and ν is the Poisson's ratio of the ice. The ice cover is modelled as a thin elastic plate within the Kirchhoff-Love plate theory [14]. The ice plate is clamped to the channel walls. The load is modelled by a localized smooth pressure distribution which moves at a constant speed U along the central line of the channel in the positive x–direction. The flow and the ice deflection are symmetric with respect to the plane $y = 0$. Initially, $t = 0$, the ice cover, the liquid and the load are at rest. The moving load causes the ice deflection around the load and may generate unsteady hydroelastic waves propagating from the load. The cases without waves in the ice cover are also studied. The flow in the channel caused by the ice deflection is potential. We shall determine the vertical displacement of the ice sheet, $w(x, y, t)$, and the stresses in it for the given characteristics of the channel, the ice cover, and the load.

The problem is formulated within the linear theory of hydroelasticity [1]. The vertical displacement of
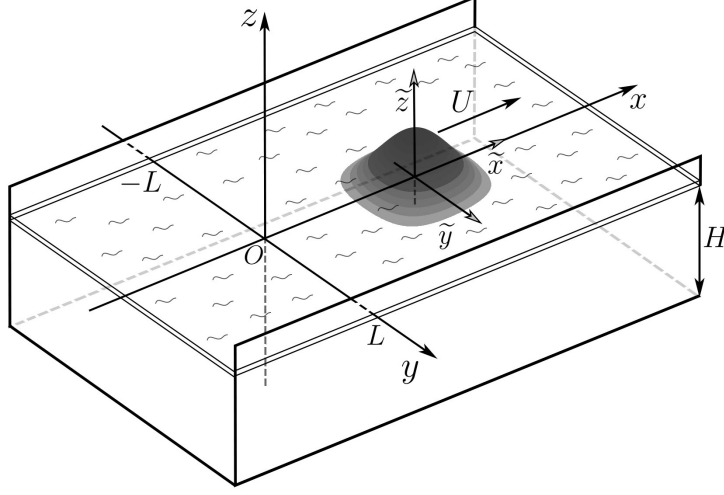
3

Figure 1: The frozen channel with the moving load.

the ice cover, $w(x, y, t)$, satisfies the equation of a thin elastic plate,

$$Mw_{tt} + D\nabla_2^4 w = p(x, y, 0, t) - P(x - Ut, y) \tag{1}$$

$$(-\infty < x < \infty, \ -L < y < L, \ z = 0),$$

where $\nabla_2^4 w = \nabla_2^2 \cdot (\nabla_2^2 w) = \partial^4 w / \partial x^4 + 2\,\partial^4 w / (\partial x^2 \partial y^2) + \partial^4 w / \partial x^4$, $M = \rho_i h_i$ is the mass of the plate per unit area, $p(x, y, 0, t)$ is the hydrodynamic pressure acting on the lower surface of the ice plate, $P(x - Ut, y)$ is the external pressure which simulates the load moving along the upper surface of the ice plate.

95   The hydrodynamic pressure, $p(x, y, 0, t)$, on the ice/water interface is given by the linearized Bernoulli equation,

$$p(x, y, 0, t) = -\rho_l\, \varphi_t(x, y, 0, t) - \rho_l g\, w(x, y, t) \tag{2}$$

$$(-\infty < x < \infty, \ -L < y < L, \ z = 0),$$

where g is the gravitational acceleration and $\varphi(x, y, z, t)$ is the velocity potential of the flow in the channel.

The velocity potential, $\varphi(x, y, z, t)$, satisfies Laplace's equation in the flow region,

$$\nabla^2 \varphi(z, y, z, t) = 0 \quad (-\infty < x < \infty, -L < y < L, -H < z < 0), \tag{3}$$

linearized kinematic condition on the ice/water interface, and the impermeability conditions on the channel

100   walls and the bottom,

$$\varphi_z = w_t \quad (z = 0), \qquad \varphi_y = 0 \quad (y = \pm L), \qquad \varphi_z = 0 \quad (z = -H). \tag{4}$$

The velocity potential decays far from the load at each finite time instant,

$$\varphi \to 0 \qquad (|x| \to \infty, \ t < \infty), \tag{5}$$

and satisfies the initial conditions,

$$\varphi = 0, \qquad \varphi_t = 0 \qquad (t = 0). \tag{6}$$

4

The positive symmetric external pressure, $P(x - Ut, y)$, acts on the upper surface of the ice plate and moves along the central line of the channel at the constant speed U, $P(x - Ut, -y) = P(x - Ut, y)$. In the coordinate system moving together with the load, (X, y, z), where $X = x - Ut$, the external pressure $P(X, y)$ does not depend on time and is described by the following equations,

$$P(x - Ut, y) = P_0 P_1\left(\frac{X}{L}\right) P_2\left(\frac{y}{L}\right) \quad (-\infty < x < \infty, -L < y < L), \tag{7}$$

$$P_1\left(\frac{X}{L}\right) = \begin{cases} \left(\cos(\pi c_1 X/L) + 1\right)/2 & (c_1|X|/L < 1), \\ 0 & (c_1|X|/L \geq 1), \end{cases}$$

$$P_2\left(\frac{y}{L}\right) = \begin{cases} \left(\cos(\pi c_2 y/L) + 1\right)/2 & (c_2|y|/L < 1), \\ 0 & (c_2|y|/L \geq 1), \end{cases}$$

in the present study, where P_0 is the magnitude of the load, $0 \leq P_1(X/L) \leq 1$, $0 \leq P_2(y/L) \leq 1$, and c_1 and c_2 are parameters of the load. Equations (7) are used only in numerical calculations. The asymptotic analysis of section 3 is valid for any integrable function $P(X, y)$.

The ice deflection $w(x, y, t)$ satisfies the clamped conditions on the channel walls,

$$w = 0, \quad w_y = 0 \quad (-\infty < x < \infty, y = \pm L), \tag{8}$$

the condition in the far field at each finite time instant,

$$w \to 0 \quad (|x| \to \infty, \ t < \infty), \tag{9}$$

and the initial conditions at $t = 0$,

$$w = w_0(x, y), \quad w_t = 0, \tag{10}$$

where $w_0(x, y)$ satisfies the static equation for a floating thin elastic plate,

$$D\nabla_2^4 w_0(x, y) = -\rho_l g \, w_0(x, y) - P(x, y), \tag{11}$$

and the conditions (8) and (9).

In the linear theory of hydroelasticity, the strains vary linearly through the ice thickness and are zero at the middle of the plate thickness. At any location, the maximum strain is achieved at the surface of the ice plate. We are concerned only with positive strains which correspond to elongations of the ice surface and tensile stresses in the ice. The strain tensor is given by

$$E(x, y) = -\zeta\frac{h_i}{2}\begin{pmatrix} w_{xx} & w_{xy} \\ w_{xy} & w_{yy} \end{pmatrix}, \tag{12}$$

where ζ is the non-dimensional coordinate across the ice thickness, $-1 \leq \zeta \leq 1$. The tensor (12) describes the strain field in the ice sheet. To find the maximum strain in the ice sheet we need to find the eigenvalues of the strain tensor at each location. The strains are proportional to the magnitude P_0 of the external load within the linear theory. The linear theory of hydroelasticity can be used when $w_x^2 + w_y^2 \ll 1$ and the strains are below the yield strain ϵ_{cr} of the ice. The yield strain of a material is defined as the strain $\epsilon = \epsilon_{cr}$ at

which a material begins to deform plastically [15]. Any strains greater than the yield strain ϵ_{cr} are assumed to lead to ice fracture. The fracture strain in experiments of [16] with ice was reported as $3 \cdot 10^{-5}$, and the theory predicts ice fracture when the strain reaches $4.3 \cdot 10^{-5}$. In this study we use the estimate $\epsilon_{cr} = 8 \cdot 10^{-5}$ (see [17] and discussion of this value there).

The solution of the unsteady problem (1) – (11) depends on the density of the liquid, ρ_l, parameters of the ice, ρ_i, h_i, D, parameters of the channel, H, L, and parameters of the load, P_0, U, c_1, c_2. We shall determine the large time behaviour of both the ice deflection, $w(x, y, t)$, and the distribution of the maximum strains in the ice plate, $\varepsilon(x, y, t)$, for some given values of the parameters of the problem. Asymptotic analysis is presented for a rectangular channel and a given form of the load (7), but it can be extended to non-rectangular channels and different distributions of the external load.

The solutions of the problem (1) – (11), where $P(X, y) = 0$ and the initial conditions and the conditions at $|x| \to \infty$ are dropped, in the forms of linear sinusoidal waves propagating along the channel were studied in [7]. The dispersion relations between the wave frequencies ω_n and the wave number k were determined numerically together with the profiles of the waves across the channel. There are infinitely many of these waves for a frozen channel, $n \geq 1$. The waves are the so-called sloshing-propagating waves. They are standing waves across the channel and propagating waves along the channel. In the coordinate system moving along the channel with the phase speed, $c_n(k) = \omega_n(k)/k$, of the n-th wave, this wave is stationary and periodic. We shall use the properties of these waves in the present analysis, to determine the asymptotic behaviour of the ice deflection, $w(x, y, t)$.

3. Ice deflection and its behaviour for large times

The Fourier transform in x,

$$w^F(\xi, y, t) = \frac{1}{\sqrt{2\pi}} \int_{-\infty}^{\infty} w(x, y, t)e^{-i\xi x}dx,$$

$$w(x, y, t) = \frac{1}{\sqrt{2\pi}} \int_{-\infty}^{\infty} w^F(\xi, y, t)e^{i\xi x}d\xi,$$

applied to the equations of the formulated problem (1) – (11) provides the plate equation,

$$Mw_{tt}^F + D\left(w_{yyyy}^F - 2\xi^2 w_{yy}^F + \xi^4 w^F\right) =$$

$$= -\rho_l \varphi_t^F(\xi, y, 0, t) - \rho_l g w^F - P^F(\xi, y)e^{-i\xi Ut}, \tag{13}$$

and the initial and boundary conditions for the deflection,

$$w^F = w_0^F(\xi, y), \quad w_t^F = 0 \quad (t = 0), \qquad w^F = 0, \quad w_y^F = 0 \quad (y = \pm L), \tag{14}$$

where $w_0^F(\xi, y)$ is the Fourier transform of the initial ice deflection, $w_0(x, y)$. The potential $\varphi^F(\xi, y, z, t)$ satisfies the modified Helmholtz equation,

$$\varphi_{yy}^F + \varphi_{zz}^F = \xi^2 \varphi^F \quad (-L < y < L, -H < z < 0), \tag{15}$$

6

and the initial and boundary conditions,

$$\varphi_z^F = w_t^F(\xi, y, t) \quad (z = 0), \qquad \varphi_y^F = 0 \quad (y = \pm L),$$

$$\varphi_z^F = 0 \quad (z = -H), \qquad \varphi^F = 0, \; \varphi_t^F = 0 \quad (t = 0). \tag{16}$$

The Fourier transform reduces the number of the independent variables by one and introduce one new parameter, which is the parameter of the transform ξ.

The ice deflection, $w^F(\xi, y, t)$, is obtained by the method of separating variables. This method separates the variables y and t:

$$w^F(\xi, y, t) = \sum_{n=1}^{\infty} a_n(\xi, t)\psi_n(\xi, y). \tag{17}$$

At this stage of the method, both functions $\psi_n(\xi, y)$ and $a_n(\xi, t)$, which also depend on the index n and the parameter ξ, are unknown and should be determined as part of the solution. The clamped conditions (14) on the wall of the channel and the symmetry of the deflection caused by the symmetric load provide

$$\psi_n(\xi, \pm L) = \psi_n'(\xi, \pm L) = 0, \quad \psi_n(\xi, -y) = \psi_n(\xi, y) \tag{18}$$

for any ξ and $|y| < L$.

The kinematic condition on the ice/water interface, $z = 0$, see the first equation in (16), suggests the following form of the velocity potential,

$$\varphi^F(\xi, y, z, t) = \sum_{n=1}^{\infty} a_{n,t}(\xi, t)\Phi_n(\xi, y, z). \tag{19}$$

The functions $\Phi_n(\xi, y, z)$ satisfy equation (15) and the boundary conditions (16), where the kinematic condition should be changed to $\Phi_{n,z}(\xi, y, 0) = \psi_n(\xi, y)$.

Substituting the series (17) and (19) in equation (13), we obtain

$$\sum_{n=1}^{\infty} a_{n,tt} \left[M\psi_n + \rho_l \Phi_n(\xi, y, 0) \right] +$$

$$+ \sum_{n=1}^{\infty} a_n \left[D \left(\psi_{n,yyyy} - 2\xi^2 \psi_{n,yy} + \xi^4 \psi_n \right) + \rho_l g \psi_n \right] = -P^F(\xi, y)e^{-i\xi Ut}. \tag{20}$$

Here the expressions in the square brackets are functions of y only. In order to separate the variables y and t in (20), these expressions are set to be proportional one to another,

$$\omega_n^2(\xi) \left[M\psi_n + \rho_l \Phi_n(\xi, y, 0) \right] = D \left(\psi_{n,yyyy} - 2\xi^2 \psi_{n,yy} + \xi^4 \psi_n \right) + \rho_l g \psi_n, \tag{21}$$

where $\omega_n^2(\xi)$ is a proportionality factor. This equation together with the conditions (18) and the corresponding equations and conditions for the functions $\Phi_n(\xi, y, z)$ form a spectral problem for the functions $\psi_n(\xi, y)$. In this problem, $\omega_n^2(\xi)$ plays a role of the spectral parameter which should be determined together with the real functions $\psi_n(\xi, y)$. The solutions of the spectral problem are known also as eigen-functions, and the spectral parameter as the eigen-value of the problem. It can be shown that the eigen-values corresponding to non-trivial eigen solutions of the formulated spectral problem are positive. This explains the notation

$\omega_n^2(\xi)$ of the eigen-values. The notation ω_n assumes that the square root of the eigen-value has a meaning of frequency. Equation (21) provides that the dimension of $\omega_n(\xi)$ is sec^{-1}, which is the dimension of frequency. The physical meaning of these frequencies will be revealed below, when we derive equations for the functions $a_n(\xi, t)$ appeared in (17). The eigen-functions $\psi_n(\xi, y)$ are numbered in such a way that the corresponding eigen-values satisfy the inequality $\omega_n < \omega_{n+1}$, where $n \geq 1$. It can be shown that the eigen-functions $\psi_n(\xi, y)$, where $n \geq 1$, are orthogonal in the following sense,

$$\int_{-L}^{L} \left[M\psi_n + \rho_l \Phi_n(\xi, y, 0) \right] \psi_m \mathrm{d}y = \delta_{nm}\sigma_n(\xi),$$

$$\sigma_n(\xi) = \int_{-L}^{L} \left[M\psi_n + \rho_l \Phi_n(\xi, y, 0) \right] \psi_n \mathrm{d}y. \tag{22}$$

In the present study, the functions $\psi_n(\xi, y)$ are normalized by the condition

$$\max_{-L < y < L} \psi_n(\xi, y) = 1. \tag{23}$$

This normalisation suggests that the functions $\psi_n(\xi, y)$ are non-dimensional. The deflection $w(x, y, t)$ and the coordinates x, y, z are measured in metres. Then in the Fourier transform, ξ is in m^{-1} and $w^F(\xi, y, t)$ in m^2. The functions $a_n(\xi, t)$ in (17) are in m^2.

The functions $\psi_n(\xi, y)$ describe the water/ice/channel system. They are independent of the load and its speed. These functions were calculated and studied in [7] in non-dimensional variables. The linear hydroelastic waves investigated in [7] are described by the equations $w(x, y, t) = A\psi_n(\xi, y) \cos[\xi x - \omega_n(\xi)t]$, where $\psi_n(\xi, y)$ is the solution of the spectral problem (21) with the spectral parameter $\omega_n^2(\xi)$, $n \geq 1$, ξ is now the wavenumber and A is the wave amplitude, in the notations of the present paper. The phase speed of the n-th wave is equal to $c^{(n)}(\xi) = \omega_n(\xi)/\xi$. The speeds $c^{(n)}(\xi)$, where $\xi \geq 0$, achieve their minimum values, $c_{\min}^{(n)} = \min_{\xi \geq 0}[c^{(n)}(\xi)]$, at single wavenumbers $\xi_{\min}^{(n)}$, where $c_{\min}^{(n+1)} > c_{\min}^{(n)}$ for $n \geq 1$. Therefore, hydroelastic waves cannot propagate at speeds less than $c_{\min}^{(1)}$. The results of [7] imply that $\omega_1(0) = 0$ and $\omega_n(0) > 0$ for $n \geq 2$. Correspondingly, $c^{(1)}(\xi)$ tends to a finite limit and $c^{(n)}(\xi)$ are unbounded as $\xi \to 0$. Only waves with $n = 1$ can propagate along the channel at speeds between $c_{\min}^{(1)}$ and $c_{\min}^{(2)}$. Typical cases are depicted in Figure 2 for particular parameters of the water/ice/channel system. For a given speed U, where $c_{\min}^{(1)} < U < c_{\min}^{(2)}$, there are two wavenumbers $\xi_1^{(1)}$ and $\xi_2^{(1)}$, $\xi_1^{(1)} < \xi_{\min}^{(1)} < \xi_2^{(1)}$, such that $c^{(1)}(\xi_1^{(1)}) = U$ and $c^{(1)}(\xi_2^{(1)}) = U$ with $c^{(n)}(\xi) > U$ for $n \geq 2$ and any ξ. In general, for $c_{\min}^{(N)} < U < c_{\min}^{(N+1)}$ with $n \geq 3$ there exist $2N - 1$ waves with wavenumbers $\xi_2^{(1)}$, $\xi_1^{(n)}$ and $\xi_2^{(n)}$, where $2 \leq n \leq N$, which propagate at speed U. There are four waves if $c_{\min}^{(2)} < U < c^{(1)}(0)$, see Figure 2.

The functions $\psi_n(\xi, y)$ are shown in Fig. 7 of the paper [7] as functions of y/L for particular characteristics of water/ice/channel system. The functions $\psi_n(\xi, y)$ and $\omega_n(\xi)$ are considered as known in the analysis below. Substituting (21) in the equation (20),

$$\sum_{n=1}^{\infty} \left(\frac{\mathrm{d}^2 a_n}{\mathrm{d}t^2} + \omega_n^2(\xi)a_n \right) \left[M\psi_n + \rho_l \Phi_n(\xi, y, 0) \right] = -P^F(\xi, y)e^{-i\xi U t}, \tag{24}$$
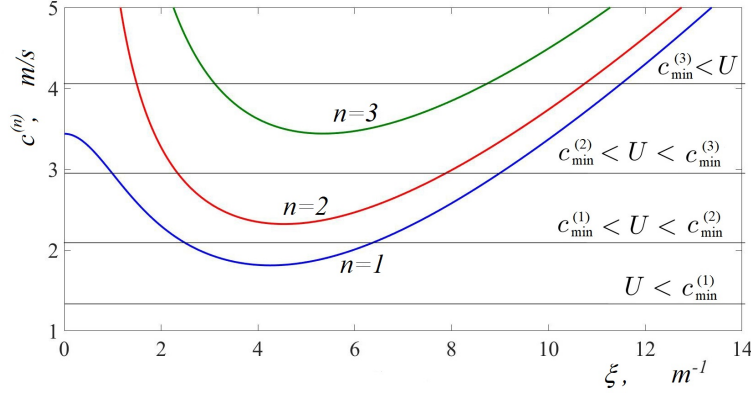
8

Figure 2: Phase speeds of even hydroelastic waves in a frozen channel. Note the number of waves propagating at different speeds U.

multiplying both sides of (24) by ψ_m, integrating the result in y from $-L$ to L, and using (22), we arrive at the infinite system of ordinary differential equations of the second order for the principal coordinates $a_n(\xi, t)$,

$$\frac{d^2 a_n}{dt^2} + \omega_n^2(\xi)a_n = H_n(\xi)e^{-i\xi U t} \qquad n = 1, 2, ...,$$

$$H_n(\xi) = -\frac{1}{\sigma_n(\xi)} \int_{-L}^{L} P^F(\xi, y)\psi_n(\xi, y)dy, \tag{25}$$

It is seen that $\omega_n(\xi)$, which were introduced in (21) as square roots of the eigen values of the spectral problem (21), are the natural frequencies of the modes $\psi_n(\xi, y)$, $n \geq 1$. The initial conditions for equations (25) follow from (14),

$$a_n(\xi, 0) = \frac{H_n(\xi)}{\omega_n^2(\xi)}, \qquad \frac{da_n}{dt}(\xi, 0) = 0. \tag{26}$$

The solution of the problem (25) – (26) reads

$$a_n(\xi, t) = \frac{\xi U H_n(\xi)}{2\omega_n^2(\xi)}\left[\frac{e^{i\omega_n t}}{\omega_n + \xi U} - \frac{e^{-i\omega_n t}}{\omega_n - \xi U}\right] + \frac{H_n e^{-i\xi U t}}{\omega_n^2 - (\xi U)^2}. \tag{27}$$

The terms in (27) are singular at $\pm\xi_1^{(n)}$ and $\pm\xi_2^{(n)}$ if the speed of the load U is large enough, $U > c_{min}^{(n)}$. Additionally, $a_1(\xi, t)$ can be singular at $\xi = 0$ because $\omega_1(\xi) = O(\xi)$ as $\xi \to 0$. However, it can be shown that $\sigma_1(\xi) = O(\xi^{-2})$ in (22) and then $H_1(\xi) = O(\xi^2)$ as $\xi \to 0$. Therefore, $a_n(\xi, t)$ have finite limits as $\xi \to 0$ for any n. Also, at any conditions, the singular terms in (27) balance each other and then the functions $a_n(\xi, t)$ are finite for any n, ξ and t.

In the moving coordinate system, $x = X + Ut$, the ice deflection, $w(X, y, t)$, is given by the inverse Fourier transform applied to series (17),

$$w(X, y, t) = \frac{1}{\sqrt{2\pi}}\sum_{n=1}^{\infty} w_n(X, y, t),$$

$$w_n(X, y, t) = \int_{-\infty}^{\infty} e^{i\xi U t}a_n(\xi, t)\psi_n(\xi, y)e^{i\xi X}d\xi. \tag{28}$$

Equations (15) and (21) show that $\psi_n(\xi, y)$, $\omega_n(\xi)$ and $\sigma_n(\xi)$ depend actually on ξ^2 and, therefore, they are even functions of the Fourier transform parameter ξ. In the present case with the external load (7) being

9

even in x, the function $H_n(\xi)$ defined in (25) is even. The integrals in the series (28) can be transformed to integrals from zero to positive infinity by using properties of the involved functions of ξ and the solution (27),

$$w_n(X, y, t) = \int\limits_{-\infty}^{0} a_n(\xi, t)\psi_n(\xi, y)e^{i\xi x}\mathrm{d}\xi + \int\limits_{0}^{\infty} a_n(\xi, t)\psi_n(\xi, y)e^{i\xi x}\mathrm{d}\xi =$$

$$= \int\limits_{0}^{\infty} H_n(\xi)\psi_n(\xi, y)\Big(\frac{2\cos(\xi X)}{\omega_n^2(\xi) - \xi^2 U^2} + \tag{29}$$

$$\frac{\xi U}{2\omega_n^2(\xi)}\Big[e^{i\xi X}\frac{e^{i(\omega_n(\xi)+\xi U)t}}{\omega_n(\xi) + \xi U} - e^{i\xi X}\frac{e^{-i(\omega_n(\xi)-\xi U)t}}{\omega_n(\xi) - \xi U} +$$

$$+ e^{-i\xi X}\frac{e^{-i(\omega_n(\xi)+\xi U)t}}{\omega_n(\xi) + \xi U} - e^{-i\xi X}\frac{e^{i(\omega_n(\xi)-\xi U)t}}{\omega_n(\xi) - \xi U}\Big]\Big)\mathrm{d}\xi.$$

The first, third and fifth terms in (29) can be singular for some values of the speed U and the mode number n but the singularities balance each other. The integrals $w_n(X, y, t)$ can be evaluated numerically for finite t providing time-dependent deflection of the ice cover. In the present study, we are concerned with the behaviour of the integrals (29) and finally the deflection (28) for large times, when $t \to \infty$ and $X = O(1)$.

The integral (29) can be decomposed into five integrals which are, in general, understood as principal value Cauchy integrals. For large n such that $c_{\min}^{(n)} > U$, these five integrals are regular with $\omega_n(\xi) \pm \xi U > 0$, where $\xi > 0$. The first integral is independent of t. The phase, $\omega_n(\xi) + \xi U$, in the second and fourth integrals is monotonic with positive derivative. By the method of integration by parts, we find that these two integrals are of order of $O(t^{-1})$ as $t \to \infty$. The phase, $\omega_n(\xi) - \xi U$, in the third and fifth integrals potentially may change the sign of its derivative in the interval, $0 < \xi < \xi_{\min}$. These integrals also decays with time but slower that $O(t^{-1})$ [18]. Finally,

$$w_n(X, y, t) = 2\int\limits_{0}^{\infty} H_n(\xi)\psi_n(\xi, y)\frac{\cos(\xi X)\mathrm{d}\xi}{\omega_n^2(\xi) - \xi^2 U^2} + o(1), \tag{30}$$

where $t \to \infty$, $c_{\min}^{(n)} > U$, and $o(1)$ stands for the terms approaching zero with increase of time t. The integrals (30) are evaluated numerically in the present study.

The asymptotic behaviour of the integral (29) as $t \to \infty$ and $X = O(1)$ is more complicated if $U > c_{\min}^{(n)}$. In this case, the equation $\omega_n(\xi) - \xi U = 0$ has two positive roots $\xi_1^{(n)}$ and $\xi_2^{(n)}$, where $\xi_1^{(n)} < \xi_{\min}^{(n)} < \xi_2^{(n)}$, see Figure 2. Note that the integrals of the second and fourth terms in (29) are not singular and their contributions are estimated as $O(t^{-1})$ as $t \to \infty$. Then (29) provides

$$w_n(X, y, t) = 2\,V.p.\!\int\limits_{0}^{\infty} H_n(\xi)\psi_n(\xi, y)\frac{\cos(\xi X)\mathrm{d}\xi}{\omega_n^2(\xi) - \xi^2 U^2} -$$

$$V.p.\!\int\limits_{0}^{\infty} H_n(\xi)\psi_n(\xi, y)\frac{\cos[\xi X - t(\omega_n(\xi) - \xi U)]}{\omega_n(\xi) - \xi U}\frac{\xi U\mathrm{d}\xi}{\omega_n^2(\xi)} + O(t^{-1}), \tag{31}$$

where *V.p.* stands for Cauchy principal value integrals. To find the asymptotic behaviour of the second Cauchy principal value integral, the interval of integration in (31) is divided into five subintervals:

$$V.p.\int_0^\infty d\xi = \int_0^{\xi_1^{(n)}-b_1^{(n)}(t)} d\xi + V.p.\int_{\xi_1^{(n)}-b_1^{(n)}(t)}^{\xi_1^{(n)}+b_1^{(n)}(t)} d\xi +$$

$$+ \int_{\xi_1^{(n)}+b_1^{(n)}(t)}^{\xi_2^{(n)}-b_2^{(n)}(t)} d\xi + V.p.\int_{\xi_2^{(n)}-b_2^{(n)}(t)}^{\xi_2^{(n)}+b_2^{(n)}(t)} d\xi + \int_{\xi_2^{(n)}+b_2^{(n)}(t)}^\infty d\xi, \tag{32}$$

where the functions $b_1^{(n)}(t)$ and $b_2^{(n)}(t)$ tend to zero together with their products with $t^{\frac{1}{2}}$, and their products with t tend to ∞ as $t \to \infty$. The first, third and fifth integrals in (32) are regular integrals approaching zero as $t \to \infty$. Asymptotic behaviours of these three integrals as $t \to \infty$ are obtained by integrating the integrals by parts. The analysis is demonstrated below for the first integral, $I^{(1)}(X, y, t)$, in (32) with the integration interval $(0, \xi_1^{(n)} - b_1^{(n)}(t))$. We introduce the regular function

$$T_n(\xi, y) = H_n(\xi)\psi_n(\xi, y)\frac{\xi - \xi_1^{(n)}}{\omega_n(\xi) - \xi U}\frac{\xi U}{\omega_n^2(\xi)},$$

which is finite in the interval $[0, \xi_1^{(n)} - b_1^{(n)}(t)]$ including its ends. Integrating $I^{(1)}(X, y, t)$ by parts, we find

$$I^{(1)}(X, y, t) = \int_0^{\xi_1^{(n)}-b_1^{(n)}(t)} \frac{T_n(\xi, y)}{\xi - \xi_1^{(n)}} \cos[\xi X - t(\omega_n(\xi) - \xi U)]d\xi =$$

$$= \int_0^{\xi_1^{(n)}-b_1^{(n)}(t)} \frac{T_n(\xi, y)}{(\xi - \xi_1^{(n)})(X - t[\omega_n'(\xi) - U])}d\{\sin[\xi X - t(\omega_n(\xi) - \xi U)]\} =$$

$$= O\left(\frac{1}{tb_1^{(n)}(t)}\right) = o(1)$$

as $t \to \infty$. Only second and fourth integrals in (32) may give non-zero contributions for large times. We shall consider the second integral. The fourth one is evaluated in a similar way. In the second integral, $I^{(2)}(X, y, t)$, we change the variable of integration to μ, where $\xi = \xi_1^{(n)} + b_1^{(n)}(t)\mu$,

$$I^{(2)}(X, y, t) = V.p.\int_{-1}^1 T_n(\xi_1^{(n)} + b_1^{(n)}(t)\mu, y) \cos[\xi X - t(\omega_n(\xi) - \xi U)]\frac{d\mu}{\mu},$$

and estimate elements of the integral for large t,

$$T_n(\xi_1^{(n)} + b_1^{(n)}(t)\mu, y) = T_n(\xi_1^{(n)}, y) + o(1),$$

$$T_n(\xi_1^{(n)}, y) = \frac{H_n(\xi_1^{(n)})\psi_n(\xi_1^{(n)}, y)}{(\omega_n'(\xi_1^{(n)}) - U)\xi_1^{(n)}U},$$

$$\xi X - t(\omega_n(\xi) - \xi U) = \xi_1^{(n)}X - \mu(\omega_n'(\xi_1^{(n)}) - U)tb_1^{(n)}(t) + o(1).$$

These estimates provide

$$I^{(2)}(X, y, t) = T_n(\xi_1^{(n)}, y)\ V.p.\int_{-1}^1 \cos[\xi_1^{(n)}X - \mu(\omega_n'(\xi_1^{(n)}) - U)tb_1^{(n)}(t)]\frac{d\mu}{\mu} + o(1) =$$

11

$$= 2T_n(\xi_1^{(n)}, y) \sin[\xi_1^{(n)} X] \int_0^1 \sin[\mu E_n(t)] \frac{\mathrm{d}\mu}{\mu} + o(1),$$

where $E_n(t) = (\omega_n'(\xi_1^{(n)}) - U)tb^{(n)}(t)$ is large as $t \to \infty$. Here

$$\int_0^1 \sin[\mu E_n(t)] \frac{\mathrm{d}\mu}{\mu} = \mathrm{sgn}(E_n) \int_0^{|E_n(t)|} \frac{\sin(\mu)\mathrm{d}\mu}{\mu} =$$

$$= \frac{\pi}{2} \mathrm{sgn}(\omega_n'(\xi_1^{(n)}) - U) + o(1),$$

where $\mathrm{sgn}(E_n) = 1$ for $E_n > 0$ and $\mathrm{sgn}(E_n) = -1$ for $E_n < 0$, and $t \to \infty$. The derivative $\omega_n'(\xi)$ is known as the group speed of the n-th mode for the wavenumber ξ. We use the notation $c_{gm}^{(n)} = \omega_n'(\xi_m^{(n)})$, where $m = 1, 2$. It can be shown that $c_{g1}^{(n)} < U$ and $c_{g2}^{(n)} > U$. Then

$$I^{(2)}(X, y, t) = -\pi T_n(\xi_1^{(n)}, y) \sin[\xi_1^{(n)} X] + o(1),$$

$$I^{(4)}(X, y, t) = \pi T_n(\xi_2^{(n)}, y) \sin[\xi_2^{(n)} X] + o(1). \tag{33}$$

Therefore, equation (31) for large times provides

$$w_n(X, y, t) = 2\, V.p. \int_0^\infty H_n(\xi)\psi_n(\xi, y) \frac{\cos(\xi X)\mathrm{d}\xi}{\omega_n^2(\xi) - \xi^2 U^2} +$$

$$+\pi T_n(\xi_1^{(n)}, y) \sin[\xi_1^{(n)} X] - \pi T_n(\xi_2^{(n)}, y) \sin[\xi_2^{(n)} X] + o(1). \tag{34}$$

Therefore, the second, time-dependent integral in (31) converges to two waves which propagate along the channel at the speed equal to the speed of the load. The formula (34) gives clear pattern of the stationary deflection w_n once the integral in it is decomposed into local and far-field response of the ice cover.

The integral in (34) is decomposed into five integrals as in (32) but now $b_j^{(n)}$, where $j = 1, 2$, are independent of time. The value of the integral in (34) is independent of the values of $b_1^{(n)}$ and $b_2^{(n)}$. The first, third and fifth integrals are regular. They are evaluated numerically and their sum is denoted by $J_n^{(R)}(X, y)$. They decay as $O(X^{-1})$, where $|X| \to \infty$, and contribute to the local deflection near the load. The second and fourth integrals are evaluated by using the definition of the Cauchy principal value integrals [19]. We introduce two regular functions,

$$R_n^{(j)}(\xi, y) = \frac{2H_n(\xi)\psi_n(\xi, y)}{\omega_n(\xi) + \xi U} \frac{\xi - \xi_j^{(n)}}{\omega_n(\xi) - \xi U},$$

where $R_n(\xi_1^{(n)}, y) = T_n(\xi_1^{(n)}, y)$. Then using the definition of Cauchy principal value integrals,

$$2\, V.p. \int_0^\infty H_n(\xi)\psi_n(\xi, y) \frac{\cos(\xi X)\mathrm{d}\xi}{\omega_n^2(\xi) - \xi^2 U^2} = \int_{\xi_1^{(n)} - b_1^{(n)}}^{\xi_1^{(n)} + b_1^{(n)}} \frac{R_n^{(1)}(\xi, y) - R_n^{(1)}(\xi_1^{(n)}, y)}{\xi - \xi_1^{(n)}} \cos[\xi X]\mathrm{d}\xi + \tag{35}$$

$$+R_n^{(1)}(\xi_1^{(n)}, y)\, V.p. \int_{\xi_1^{(n)} - b_1^{(n)}}^{\xi_1^{(n)} + b_1^{(n)}} \frac{\cos[\xi X]\mathrm{d}\xi}{\xi - \xi_1^{(n)}} + \int_{\xi_2^{(n)} - b_2^{(n)}}^{\xi_2^{(n)} + b_2^{(n)}} \frac{R_n^{(2)}(\xi, y) - R_n^{(2)}(\xi_2^{(n)}, y)}{\xi - \xi_2^{(n)}} \cos[\xi X]\mathrm{d}\xi +$$

$$+R_n^{(2)}(\xi_2^{(n)}, y)\, V.p. \int_{\xi_2^{(n)} - b_2^{(n)}}^{\xi_2^{(n)} + b_2^{(n)}} \frac{\cos[\xi X]\mathrm{d}\xi}{\xi - \xi_2^{(n)}} + J_n^{(R)}(X, y).$$

12

The first and third integrals in (35) are regular. They decay as $O(X^{-1})$, where $|X| \to \infty$, and contribute to the local deflection near the load similar to the term $J_n^{(R)}(X, y)$. These two integrals are evaluated numerically and their sum with $J_n^{(R)}(X, y)$ is denoted by $w_n^{(loc)}(X, y)$, see (31). Note that $w_n^{(loc)}(X, y)$ is an even function of X and y, and it decays as $O(X^{-1})$ with the distance from the load, where $|X| \to \infty$. The Cauchy principal value integrals in (35) are evaluated by using the substitution $\xi = \xi_j^{(n)} + b_j^{(n)}\sigma$, where $j = 1, 2$,

$$V.p. \int_{\xi_j^{(n)} - b_j^{(n)}}^{\xi_j^{(n)} + b_j^{(n)}} \frac{\cos[\xi X] \mathrm{d}\xi}{\xi - \xi_j^{(n)}} = V.p. \int_{-1}^{1} \cos[\xi_j^{(n)} X + b_j^{(n)} X\sigma] \frac{\mathrm{d}\sigma}{\sigma} =$$

$$- \sin[\xi_j^{(n)} X] \int_{-1}^{1} \sin[b_j^{(n)} X\sigma] \frac{\mathrm{d}\sigma}{\sigma} = -2\sin[\xi_j^{(n)} X]\mathrm{sgn}(X) \int_0^{b_j^{(n)}|X|} \sin(u) \frac{\mathrm{d}u}{u} \qquad (36)$$

Substituting equations (35), (36) and the functions $R_n^{(j)}(\xi_j^{(n)}, y)$ and $T_n(\xi_j^{(n)}, y)$ in (34), we obtain the deflection $w_n(X, y, t)$ for large times t as the sum of the deflection $w_n^{(loc)}(X, y)$ localised near the load and two waves propagating from the load,

$$w_n(X, y, t) = w_n^{(loc)}(X, y) - A_1^{(n)} \psi_n(\xi_1^{(n)}, y) \sin[\xi_1^{(n)} X] G_1^{(n)}(X) -$$

$$- A_2^{(n)} \psi_n(\xi_2^{(n)}, y) \sin[\xi_2^{(n)} X] G_2^{(n)}(X), \qquad (37)$$

$$A_j^{(n)} = \frac{2\pi H_n(\xi_j^{(n)})}{(\omega_n'(\xi_j^{(n)}) - U)\xi_j^{(n)} U} \quad (j = 1, 2), \qquad (38)$$

$$G_1^{(n)}(X) = \frac{1}{\pi}\mathrm{sgn}(X) \int_0^{b_1^{(n)}|X|} \frac{\sin(u)\mathrm{d}u}{u} - \frac{1}{2},$$

$$G_2^{(n)}(X) = \frac{1}{\pi}\mathrm{sgn}(X) \int_0^{b_2^{(n)}|X|} \frac{\sin(u)\mathrm{d}u}{u} + \frac{1}{2}. \qquad (39)$$

The products $\psi_n(\xi_1^{(n)}, y) \sin[\xi_1^{(n)} X]$ and $\psi_n(\xi_2^{(n)}, y) \sin[\xi_2^{(n)} X]$ in (37) correspond to the n-th mode of the wave propagating along the frozen channel. The wavenumbers of these waves are such that their phase speeds are equal to the speed of the load U. The absolute values of $A_1^{(n)}$ and $A_2^{(n)}$ given by (38) are the amplitudes of these waves. The amplitude $A_j^{(n)}$ tends to infinity when the group speed $\omega_n'(\xi_j^{(n)})$ approaches the speed of the load, U. For such a wavenumber ξ, the phase speed and the group speed are equal, which is possible only at the wavenumber for which the phase speed is minimum. This is, for the speed of the load being equal to the critical speed of the n-th wave. The linear theory of hydroelasticity without damping is not valid for the critical speeds of the load motions. The cut-off function $G_1^{(n)}(X)$ tends to minus one as $X \to -\infty$ and to zero as $X \to +\infty$. The function $G_2^{(n)}(X)$ tends to one as $X \to +\infty$ and to zero as $X \to -\infty$. Note that these functions depend on $b_1^{(n)}$ and $b_2^{(n)}$, correspondingly. Therefore, the long wave, $A_1^{(n)} \psi_n(\xi_1^{(n)}, y) \sin[\xi_1^{(n)} X] G_1^{(n)}(X)$, exists behind the load and the short wave, $A_2^{(n)} \psi_n(\xi_2^{(n)}, y) \sin[\xi_2^{(n)} X] G_2^{(n)}(X)$ is in front of the load. Both waves are stationary in the system moving together with the load at speed U.

The total deflection of the ice cover is the sum of the contributions from each mode, see (28). The contributions of higher modes with $c_{\min}^{(n)} > U$ are the localised and even in x deflections (30) without waves. Each mode with $c_{\min}^{(n)} < U$ contributes two waves, see (37), in addition to the localised contribution

13

$w_n^{(loc)}(x, y)$, except of the lowest mode with $n = 1$ for which the long wave behind the load can be missing, see Figure 2 for explanations. The local contributions, $w_n^{(loc)}(X, y)$, are calculated numerically for $n \geq 1$.

The large-time asymptotic solution (28), (37) is for a load of a constant magnitude moving along the channel at a constant speed. If the load is time dependent, then $H_n(\xi, t)$ in (25) depends on time. If the speed of the load is time-dependent, then the power of the exponent in (25), $-i\xi Ut$, should be changed to $-i\xi s(t)$, where $s(t)$ is the distance travelled by the load. In general, the problem of time-dependent moving load and the strain field caused by such a load are complex and difficult to analyse. Some progress can be achieved for oscillating magnitude of the load,

$$P_0(t) = P_{00}(1 + A\cos(\omega' t)), \tag{40}$$

where ω' is the frequency and A is the relative amplitude of the oscillations, see [20]. It is convenient to show the dependence of the solution (27) on the speed U and the load magnitude $P_0(t)$ explicitly, $a_n(\xi, t, U, P_0)$, and notice that ξ is a parameter of the solution. Then the solution of the problem with the time-oscillating load (40) can be obtained as the following combination of the solutions (27),

$$a_n(\xi, t, U, P_0(t)) = a_n(\xi, t, U, P_{00}) +$$

$$+ \frac{1}{2}A\{a_n(\xi, t, U - \omega'/\xi, P_{00}) + a_n(\xi, t, U + \omega'/\xi, P_{00})\}. \tag{41}$$

The first term in (41) provides to the large-time deflections (37). The second and third terms are proportional to the relative amplitude of the oscillation A and describe new systems of waves, which are not stationary in the moving coordinate system. These waves prorogate from the load at the relative speeds $\pm\omega'/\xi$. Each term in (41) contributes to the localised deflection in the place of the load as $t \to \infty$.

In the problem of the load of constant magnitude P_0 moving at time dependent speed $U(1 + \varepsilon\sin(\omega' t))$ which oscillates with a relatively small amplitude εU and frequency ω', the distance travelled by the load is

$$s(t) = Ut - \varepsilon\frac{U}{\omega'}\cos(\omega' t).$$

Then the right hand side in (25) reads

$$H_n(\xi)\exp\left\{-i\xi(Ut - \varepsilon\frac{U}{\omega'}\cos(\omega' t)\right\} \approx$$

$$\approx H_n(\xi)e^{-i\xi Ut}\left\{1 + \varepsilon\, i\xi\frac{U}{\omega'}\cos(\omega' t) + O(\varepsilon^2)\right\}$$

and can be interpreted as that one for a time-dependent load with the magnitude (40), where $A = i\xi U\varepsilon/\omega'$. Then the decomposition (41) can be approximately used for the load moving with the oscillating speed. Note that we do not consider here the critical conditions of the motion, when the linear theory of hydroelastic waves is not applicable.

4. Numerical results

Calculations are performed for the laboratory ice tank at the Sholem Aleichem Amur State University. The length of the tank is 14 m. The tank is 1 m deep, $H = 1$ m, and 3 m wide, $L = 1.5$ m, with a typical

14

ice thickness $h_i = 3$ mm (see [21]). The water density is equal to $\rho_l = 1024$ kg/m³, and the ice density is $\rho_i = 920$ kg/m³. The Young modulus is taken as $E = 4.2 \cdot 10^9$ N/m² and Poisson's ratio as $\nu = 0.33$. The rigidity of this ice sheet is $D = 10.6$ Nm and the characteristic length of the sheet is $L_c = (D/\rho g)^{\frac{1}{4}} \approx 18$ cm. The external load (7) is applied over the square 20×20 cm, which gives $c_1 = c_2 = 15$, moving along the centre line of the tank.

The tank is infinitely long in the present calculations. Only even in y modes are considered. The calculated phase speeds, $c^{(n)}(\xi)$, for $n = 1, 2, 3$ are shown in the Figure 2. Here $c_{\min}^{(1)} = 1.81$ m/s, $c_{\min}^{(2)} = 2.321$ m/s and $c_{\min}^{(3)} = 3.446$ m/s. The phase speed for the first mode and long waves is $c^{(1)}(0) = 3.44$ m/s, which should be compared with the critical speed of water waves in the tank, $\sqrt{gH} = 3.13$ m/s. It is seen that long hydroelastic waves propagate at slightly higher speed than the water waves without the ice cover. This effect is due to the rigidity of the ice cover and the presence of the side walls of the channel. Note that there is a single phase speed of flexural-gravity waves without the side walls, which approaches the critical speed of waves in open water for long waves.

The elements of the large-time deflection in the coordinate system moving together with the load are analysed for the load magnitude $P_0 = 100$ N/m² and the speed of the load $U = 2$ m/s. For this speed of the load, only the waves corresponding to the first even mode are generated, see Figure 2 and equations (30) and (37). The wavenumbers of the corresponding waves of the first mode, which phase speeds are equal to the speed of the load, are $\xi_1^{(1)} = 2.77$ m⁻¹ and $\xi_2^{(1)} = 5.96$ m⁻¹. These wavenumbers correspond to wavelength of 2.29 and 1.06 m. The critical speed of the first wave mode is achieved at $\xi_{\min}^{(1)} = 4.25$ m⁻¹. The group speeds of the generated waves are $c_{g1}^{(1)} = 1.23$ m/s and $c_{g2}^{(1)} = 3.22$ m/s. The amplitudes of these waves are given by (38) and are equal to $|A_1^{(1)}| = 9.66 \cdot 10^{-4}$ m and $|A_2^{(1)}| = 5.83 \cdot 10^{-4}$ m. Note that the dimension of $H_n(\xi)$ is m²/s². Here $A_1^{(1)}$ is positive and $A_2^{(1)}$ is negative. The local contributions of the even modes, $w_n^{(loc)}(X, y)$, to the total deflection are shown in Figure 3 for for centre line of the channel, $y = 0$. These contributions are even in X and quickly decay with the mode number.
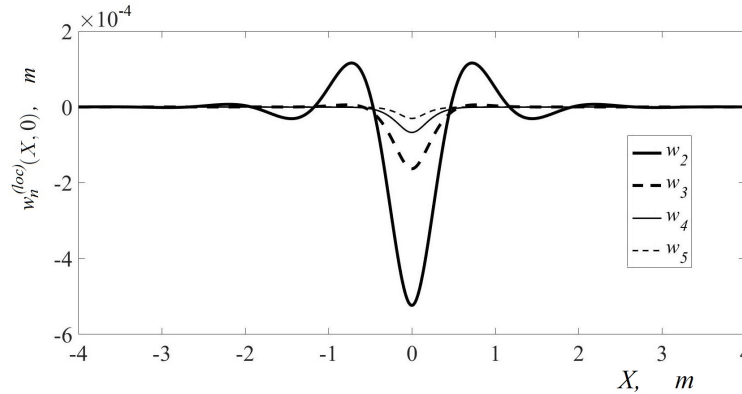

Figure 3: Contributions of the second, third, fourth and fifth modes to the total deflection.

The cut-off functions $G_{1,2}^{(1)}(x)$, see (39), for two cases, $b_1^{(1)} = b_2^{(1)} = 0.5$ and $b_1^{(1)} = b_2^{(1)} = 1.5$, and the local contribution of the first mode, $w_1^{(loc)}(X, 0)$, for these two cases are depicted in Figs. 4 and 5. Note that the constants $b_1^{(1)}$ and $b_2^{(1)}$ in (39) are very different in those cases resulting in different elements of the
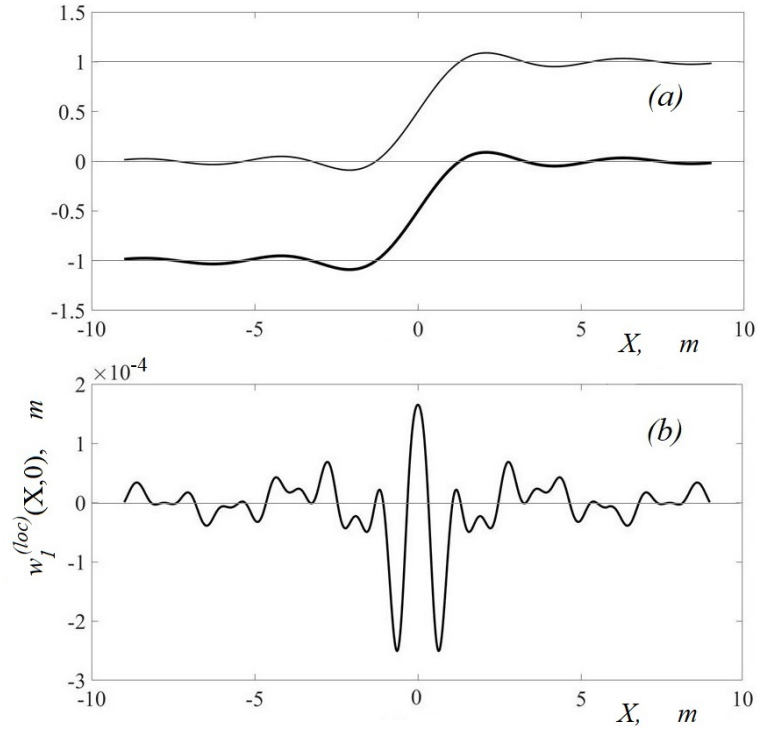
Figure 4: (a) Cut-off functions $G_{1,2}^{(1)}(x)$ given by (39) for $b_1^{(1)} = b_2^{(1)} = 0.5$. Thick lines are for the long wave behind the load, $G_1^{(1)}(x)$, and the thin lines are for short wave in front of the load, $G_2^{(1)}(x)$. (b) Corresponding contribution $w_1^{(loc)}(X,0)$.
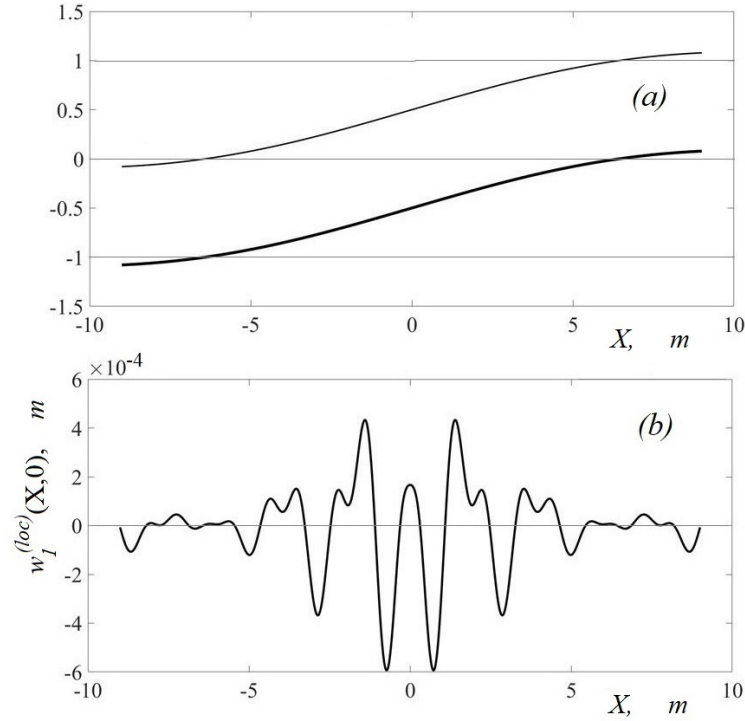

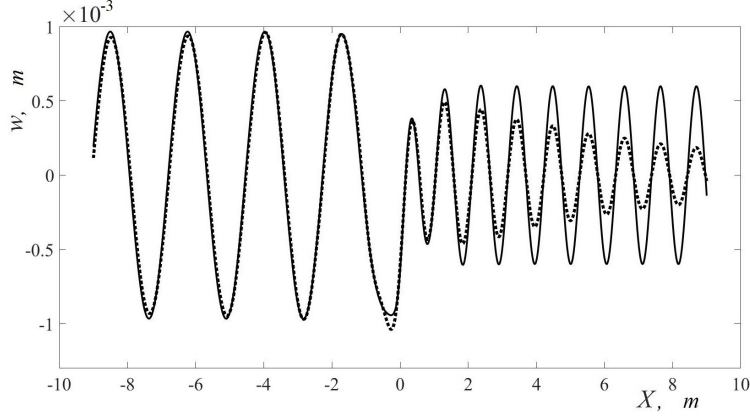Figure 5: The same as Fig. 4, but for $b_1^{(1)} = b_2^{(1)} = 1.5$.

Figure 6: The total deflection of the ice by the present analysis along the centre line of the channel, $y = 0$, near the moving load for large times with $P_0 = 100 \text{N/m}^2$ (solid line). The corresponding deflection by the visco-elastic model of ice [8] with the retardation time $\tau = 0.004$ s is shown by the dotted line.

first-mode contribution. However the total deflection (28) along the centre line of the channel is the same, see the solid lines in Fig. 6, as expected. The dotted line in Fig. 6 shows the ice deflection at the centre line predicted for the same load by the visco-elastic ice model from [8] with the retardation time $\tau = 0.004$ s. It is seen that the deflection predicted by the present analysis without dissipation agrees with the visco-elastic solution very well. In the visco-elastic model, the short waves in front of the load decay quicker than the longer waves behind the load.

The large-time strain distribution over the ice cover scaled with the yield strain of the ice, ϵ_{cr}, is shown in Fig. 7 as a contour plot (a) and 3D plot (b). It is seen that the strains are maximum in front of the load at the centre line of the channel.

The directions of the maximum strains on the ice surface at different points are shown in Fig. 8. If the local maximum strain at a point exceeds the yield strain, ϵ_{cr}, then a crack may appear at this location being perpendicular to the shown direction. Possible cracks are parallel to the walls in the close proximity of the wall and are perpendicular to the direction of the load motion far from the walls.

Fig. 7 shows that the maximum strains occur at the centre line of the channel in front of the moving load. The strains far from the load are described by the wave components given by the second and third terms in (37). By using these wave components, we can readily calculate the maximum strains at different locations across the channel for different loads and different speeds, see Fig. 9. This figure shows the scaled maximum strains for the load (7) and speed of its motion from the critical speed of the first mode to the critical speed of the third mode. The linear theory of hydroelasticity predicts unbounded strains for the critical speeds. It is interesting to note that the strains at the centre line in front of the load are always greater that the strains on the wall. However, behind the load, the strains on the wall are greater than at the centre line. The strains in front of the load are greater than behind the load even the amplitude of the long wave behind the load is higher than the amplitude of the short wave in front of the load, see Fig. 7. Therefore, the model of ice without dissipation predicts that the ice always breaks in front of the load. Even small dissipation, see Fig. 7, significantly reduces the strains in front of the load.
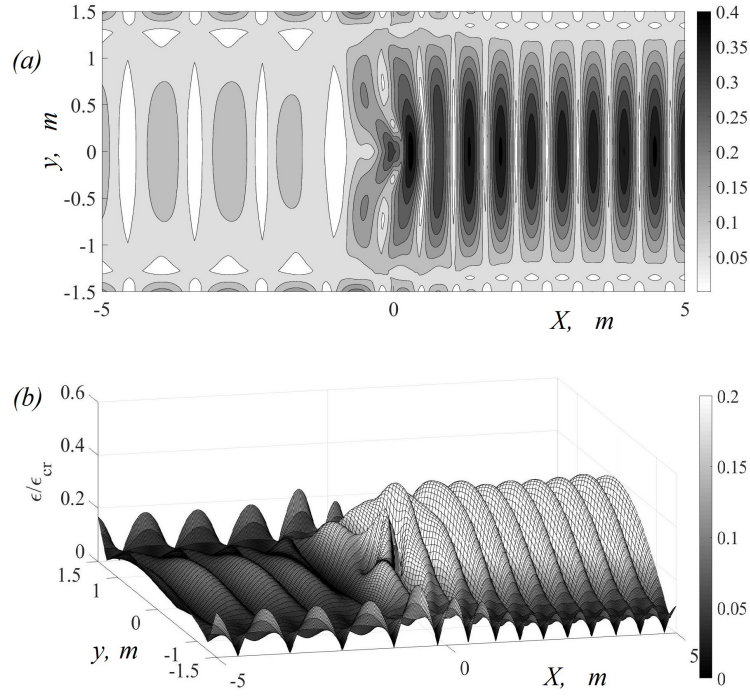
17

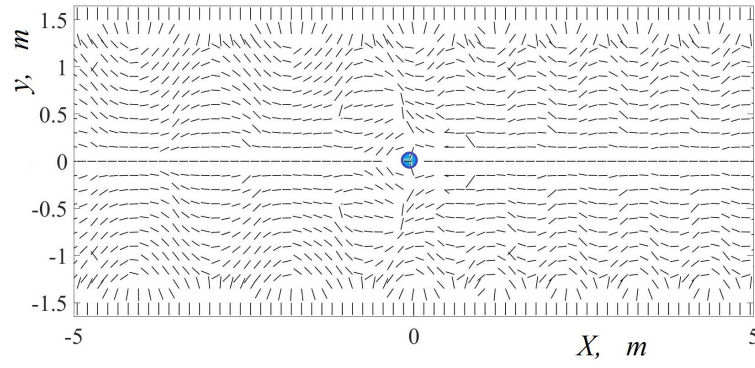Figure 7: Strain distribution over the ice cover.

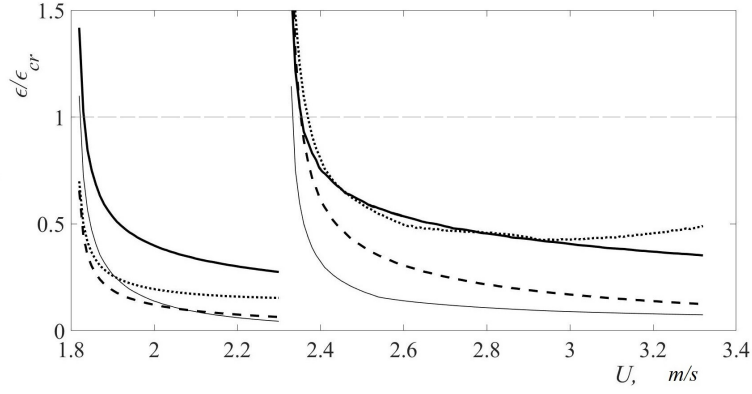Figure 8: Directions of maximum strains over the ice cover.

Figure 9: The scaled strain maxima far from the load at different locations as functions of the load speed starting from the lowest critical speed. The maximum strain far ahead the load at the centre of the channel is shown by the thick solid line, and on the wall by dashed line. The maximum strain far behind the load at the centre of the channel is shown by the thin solid line, and on the wall by dotted line.

The deflection of the ice cover for the speeds of the load below the first critical speed are shown in Fig. 10 together with the strains along the centre line of the channel and the walls. The figure confirms that the deflections quickly decay with the distance from the load. Both the deflections and strains increase when the load speed approaches the first critical speed from below. Even there are no wave components in the deflection for subcritical speeds, the deflection approaches the wave form with the wavenumber of the critical speed of the first mode, $\xi_{\min}^{(1)} = 4.25$ 1/m. Note that only the absolute values of the strains are shown in the figures.
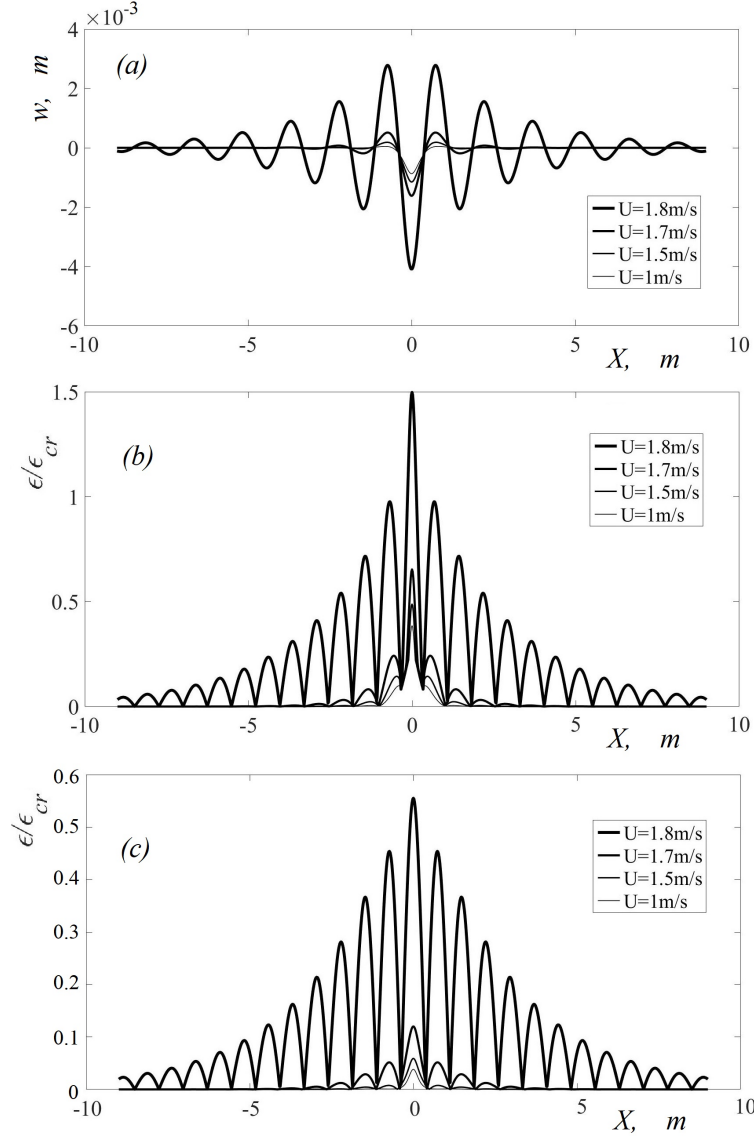
19

Figure 10: Distributions of ice deflections and strains in the ice plate for subcritical speeds of the load: (a) deflection of the ice cover along the centre line of the channel, (b) scaled strain along the centre line of the channel, (c) scaled strain along the wall of the channel.

5. Conclusion

Large time asymptotic solution of three-dimensional problem of hydroelasticity for a channel covered with ice sheet has been studied. The deflection of the ice cover is caused by a load moving along the centre line of the channel at a constant speed. The ice sheet is clamped to the vertical walls of the channel in this study. It has been shown that the ice response strongly depend on the speed of the load and the value of the speed with respect to the critical speeds of the flexural-gravity waves propagating along the channel. These waves were studied in [7]. It was shown that, for the speed of the load below the lowest critical speed, the ice response to the moving load is localised near the load. When the load speed approaches the lowest critical speed, the ice response grows in magnitude and exhibits hydroelastic wave corresponding to the lowest mode with the length at which the phase speed of this wave is minimum. The present linear analysis does not work for the load speed close to a critical speed of the hydroelastic waves in the channel. For the load speed greater than the lowest critical speed but below the second critical speed, two systems of waves are formed in front and behind the moving load. Both waves propagate at the phase speed equal to the speed of the load. The wave in front of the load is shorter and the wave behind the load is longer than the wave of the lowest critical speed.

The short wave in front of the load has smaller amplitude but larger curvature than the longer wave behind the load. The asymptotic analysis of the ice response, which is valid for long time after the load started its motion, provides the structure of the ice deflection near and far from the load. The large-time ice response consists of the symmetric response localised near the load and two wave systems modulated by smooth cut-off functions. The amplitudes of the waves in the far field were obtained analytically, which simplifies the calculations of ice deflection and strain distributions at a distance from the load.

Once the load speed increases further, it becomes greater than the second critical speed. Then two new wave system corresponding to the second mode of hydroelastic propagating waves appear in addition to the existing systems. The number of waves behind and in front of the load has been obtained for any speed of the load.

The distribution of strains in the ice cover has been investigated. It was concluded that the ice breaks in front of the moving load at the centre of the channel. This conclusion is valid for ice sheets with relatively small dissipation, when waves generated by the load can be observed well ahead of the load. Behind the load, the strains are maximum on the vertical walls of the channel and are relatively low close to the centre of the channel.

The obtained results without account for any dissipation are in good agreement with the results obtained earlier [8] within the Kelvin-Voight model of visco-elastic ice, when the retardation time is small. The ice deflection and strains are difficult to compute numerically by this visco-elastic model for small dissipation but can be easily estimated within the asymptotic analysis of this study. The strains computed without account for dissipation effects are larger than actual strains. They can be used to estimate conditions of safe transportation along frozen channels.

The load moves along the central line of the channel in this paper. One can expect that the strain in the ice cover are smaller, where the load moves closer to one of the channel walls. Therefore, the present

estimates of the bearing capacity of the ice cover in the channel could provide the upper bound of strains for any distance of the load motion from the walls. This problem should be carefully investigated in the future studies of hydroelastic waves.

Acknowledgement

[1] V. Squire, R. Hosking, A. Kerr and P. Langhorne (1996). Moving loads on ice plates. Kluwer Academic Publishers; 1996.

[2] P. Guyenne, E. Parau (2012). Computations of fully nonlinear hydroelastic solitary waves on deep water. Journal of Fluid Mechanics, 713, 307-329.

[3] R.J. Hosking, A.D. Sneyd D.W. and Waugh (1988). Viscoelastic response of a floating ice plate to a moving load. Journal of Fluid Mechanics, 196, 409-430.

[4] Tabata T. Studies on visco-elastic properties of sea ice. In Arctic Sea Ice. US National Academy of Sciences & National Research Council (Washington, DC), publication 598, pp. 139-147.

[5] Kozin VM, Zhestkaya VD, Pogorelova AV, Chizhumov SD, Dzhabailov MP, Morozov VS, Kustov AN. Applied problems of the dynamics of ice cover (in Russian). Academy of Natural Sciences, Moscow; 2008.

[6] Zhestkaya VD, Kozin VM. Ice Breaking with Air-Cushion Vessels Using a Resonant Method. Dalnauka, Vladivostok; 2003; 160pp.

[7] A. Korobkin, T. Khabakhpasheva and A. Papin (2014). Waves propagating along a channel with ice cover. European Journal of Mechanics - B/Fluids, 47, 166-175.

[8] K. Shishmarev, T. Khabakhpasheva and A. Korobkin (2016). The response of ice cover to a load moving along a frozen channel. Applied Ocean Research, 59, 313-326.

[9] R. Schulkes and A. Sneyd (1988). Time-dependent response of floating ice to a steadily moving load. Journal of Fluid Mechanics, 186, 25-46.

[10] A. Korobkin, T. Khabakhpasheva (1998). Plane problem of asymmetrical wave impact on an elastic plate Journal of Applied Mechanics and Technical Physics 39 (5), 782-791.

[11] A. Korobkin (2000). Unsteady hydroelasticity of floating plates. Journal of Fluids and Structures, 14(7), 971-991.

[12] T. Khabakhpasheva (2006). Impact of a surface wave on an elastic hull. Fluid Dynamics, 41(3), 424-433.

[13] E.A.Batyaev and T.I. Khabakhpasheva (2015). Hydroelastic waves in a channel covered with a free ice sheet. Fluid Dynamics, 50(6), 775-788.

[14] Timoshenko, S. and Woinowsky-Krieger, S. Theory of Plates and Shells. 2nd ed., McGraw-Hill, New York, U.S.A., 1959.

[15] Jones F, Ryffel H, Oberg E, McCauley C. Machinerys handbook. 27th edn, Industrial Press Inc, New York; 2004.

[16] Goodman D, Wadhams P, Squire V. The flexural response of a tabular ice island to ocean swell. Ann Glaciol 1980;1:237.

[17] Brocklehurst P, Korobkin AA, Părău EI. Interaction of hydro-elastic waves with a vertical wall. J Eng Math 2010;68:215–31.

[18] Erdelyi A. Asymptotic expansions. New York: Dover Publications, Inc., 1956.

[19] Gakhov F.D. Boundary Value Problems. Pergamon press. 1966.

[20] Shishmarev K.A., Khabakhpasheva T.I. and Korobkin A.A. The ice response to an oscillating load moving along a frozen channel. IOP Conference Series: Earth and Environmental Science 2018;193:012072

[21] Zemlyak V.L., Kozin V.M., Baurin N. O., Ipatov K. I. The Research on Deformed State of Hummocked Ice Caused by Motion of a Submarine Vessel. Proceedings of the Twenty-seventh International Ocean and Polar Engineering Conference San Francisco, CA, USA, June 25-30, 2017. 1332–1337.